Nuclear Science and Techniques (2024) 35:91
https://doi.org/10.1007/s41365-024-01450-0

Improved nuclear mass formula with an additional term from the Fermi gas model

Xiao-Yu Xu[1] · Li Deng[1] · Ai-Xi Chen[1] · Hang Yang[1] · Amir Jalili[1] · Han-Kui Wang[1]

Received: 22 December 2023 / Revised: 19 January 2024 / Accepted: 10 February 2024 / Published online: 3 June 2024

Abstract
Nuclear mass is a fundamental property of nuclear physics and a necessary input in nuclear astrophysics. Owing to the complexity of atomic nuclei and nonperturbative strong interactions, conventional physical models cannot completely describe nuclear binding energies. In this study, the mass formula was improved by considering an additional term from the Fermi gas model. All nuclear masses in the Atomic Mass Evaluation Database were reproduced with a root-mean-square deviation (RMSD) of ~1.86 MeV (1.92 MeV). The new mass formula exhibits good performance in the neutron-rich nuclear region. The RMSD decreases to 0.393 MeV when the ratio of the neutron number to the proton number is ≥1.6.

Keywords Nuclear mass formula · Neutron-rich nuclei · Fermi-gas model

1 Introduction

The precise calculation of the nuclear mass is of profound significance in the fields of nuclear physics and astrophysics [1]. Nuclear physics encompasses the analysis of over 3,000 measured nuclear masses, enabling the exploration of nuclear symmetry energy [2–5]. Synthesis of superheavy nuclei [6–8] has attracted increasing attention in recent years [9]. Accurate predictions of shell corrections and α-decay energies of superheavy nuclei are urgently required to synthesize new superheavy nuclei [10]. Concurrently, nuclear symmetry energy is believed to be crucial for correctly interpreting nuclear masses [9, 11], influencing both the nuclear structure and dynamic behavior of nuclear reactions [10]. Several nuclear mass models have been developed to achieve root-mean-square deviations (RMSDs) ranging from several hundred keV to a few MeV for all known nuclear masses.

Unmeasured masses are typically predicted by using global nuclear mass models that incorporate various physical aspects. The model parameters are determined either by employing the available measured masses [12–15] or by adopting local mass relations based on the measured masses of neighboring nuclei. Global nuclear mass models, such as the finite range droplet model (FRDM) [12, 16], extended Bethe–Weizsäcker (BW2) formula [17], Weizsäcker–Skyrme (WS) mass models [2, 9, 10], nonrelativistic Hartree–Fock–Bogoliubov (HFB) approach with the Skyrme energy-density functional (EDF) [18], Gogny forces and the relativistic mean-field (RMF) model [19], and Duflo–Zuker (DZ) mass models [20], successfully reproduce measured masses with an accuracy at the level of 300–600 keV. Although the predictions from these global mass models closely align with known masses, substantial differences arise when addressing neutron drip lines and superheavy nuclei. These differences highlight the need to consider additional physics and information regarding nuclear forces in mass models for accurate predictions in these regions.

In addition to global mass models, local mass relations such as the isobaric multiplet mass equation (IMME) [21], Garvey–Kelson (GK) relations [22–24], and residual proton–neutron interactions [25–27] can be employed to predict unmeasured masses. However, it has been observed that

This work was supported by the National Natural Science Foundation of China (Nos. 12175199 and U2267205) and a ZSTU intramural grant (No. 22062267-Y).

✉ Li Deng
lideng75@zstu.edu.cn

✉ Ai-Xi Chen
aixichen@zstu.edu.cn

✉ Han-Kui Wang
whk2007@163.com

[1] School of Science, Zhejiang Sci-Tech University, Hangzhou 310018, China

using these local mass relations to iteratively predict masses leads to a rapid increase in the intrinsic error [28]. This is attributed to two main factors: 1. The local mass relations are only approximately satisfied for known masses and 2. the previously predicted masses are incorporated in each new iteration, resulting in the accumulation of systematic error [29]. The mass relations of mirror nuclei operate under the assumption that nuclear interactions conserve isospin symmetry [30–32]. Recently, these relationships were proven to be remarkably accurate. Under this assumption, the mass difference between the two mirror nuclei is determined by the Coulomb interaction and constant values associated with the neutron–proton mass difference [31].

Recently, artificial neural networks (ANNs), one of the most powerful machine-learning methods, have been successfully applied in nuclear physics studies [33–37]. In nuclear physics, Bayesian neural networks (BNNs) have been employed to minimize mass residuals between theory and experiment. There has been notable enhancement in the mass prediction of several theoretical models following BNN refinement [38–40]. For instance, the RMSD of the liquid-drop model decreases from ~3 to ~0.8 MeV.

This study focused on improving the BW2 mass formula, with attention directed toward the Fermi gas model [41] and higher order term of the symmetry energy [42–44]. The results indicate that the RMSD of the modified BW2 mass formula was reduced by 3%, representing a significant improvement in the accuracy of calculating neutron-rich nuclei [45–49].

The remainder of this paper is organized as follows. Section 2 provides an explanation of the BW2 mass formula and the derivation of the correction term. The results and discussion are presented in Sect. 3, and a summary and future prospects are provided in Sect. 4.

2 Nuclear mass model

2.1 Mass formula

The mass formula BW2 is based on the classical liquid-drop model and incorporates additional physical terms for a more comprehensive analysis. In this formula, the exchange Coulomb term $\alpha_{\mathrm{xC}}\frac{Z^{\frac{4}{3}}}{A^{\frac{1}{3}}}$, Wigner term $\alpha_{\mathrm{W}}\frac{|N-Z|}{A}$, surface symmetry term $\alpha_{\mathrm{st}}\frac{(N-Z)^2}{A^{\frac{4}{3}}}$, pairing term $\alpha_{\mathrm{p}}\frac{\delta(N,Z)}{A^{\frac{1}{2}}}$, curvature term $\alpha_{\mathrm{R}}A^{\frac{1}{3}}$, and shell effect term $\alpha_{\mathrm{m}}P+\beta_{\mathrm{m}}P^2$ have been added. It should be noted that the shell effect term contains two parameters. The model used in this study is obtained from Refs. [17]:

$$\begin{aligned} BE_{\mathrm{BW2}} =& \alpha_{\mathrm{v}}A+\alpha_{\mathrm{s}}A^{\frac{2}{3}}+\alpha_{\mathrm{C}}\frac{Z^2}{A^{\frac{1}{3}}}+\alpha_{\mathrm{t}}\frac{(N-Z)^2}{A} \\ &+\alpha_{\mathrm{xC}}\frac{Z^{\frac{4}{3}}}{A^{\frac{1}{3}}}+\alpha_{\mathrm{W}}\frac{|N-Z|}{A}+\alpha_{\mathrm{st}}\frac{(N-Z)^2}{A^{\frac{4}{3}}} \\ &+\alpha_{\mathrm{p}}\frac{\delta(N,Z)}{A^{\frac{1}{2}}}+\alpha_{\mathrm{R}}A^{\frac{1}{3}}+\alpha_{\mathrm{m}}P+\beta_{\mathrm{m}}P^2, \end{aligned} \tag{1}$$

where α_i denotes the free parameters determined by fitting the experimental nuclear masses. $\delta(N,Z)$ is given by

$$\delta(N,Z)=\frac{(-1)^N+(-1)^Z}{2}; \tag{2}$$

that is, $\delta(N,Z)$ takes the value +1 for even–even nuclei, −1 for odd–odd nuclei, and 0 for odd nuclei. P is given by

$$P=\frac{\nu_{\mathrm{n}}\nu_{\mathrm{p}}}{\nu_{\mathrm{n}}+\nu_{\mathrm{p}}}, \tag{3}$$

where ν_{n} and ν_{p} are the number of valence nucleons (the difference between the actual nucleon numbers N and Z and the nearest magic numbers, respectively). To calculate P, the magic numbers were canonical 2, 8, 20, 28, 50, 82, 126, and 184 for both neutrons and protons.

The latest and most comprehensive database of nuclear masses is the Atomic Mass Evaluation Database, commonly known as AME2020 [50]. This tabulation served as the experimental data for this study. The pertinent input comprises a list of the measured binding energies of the nuclei acquired by multiplying the tabulated binding energy per nucleon by the mass number (A).

2.2 Improved nuclear mass formula

In this section, we demonstrate that the nucleon binding energies can be understood using the Fermi gas model. Moreover, the primary terms of the semiempirical mass formula arise naturally from the model. Protons and neutrons, including the nucleus, are conceptualized in the Fermi gas model to form two independent nucleon systems. It is assumed that the nucleons can move freely throughout the entire nuclear volume within the constraints imposed by Pauli's principles. The potential participating in each nucleon is a superposition of the potentials generated by other nucleons.

A system of such fermions is treated as a degenerate gas, and its temperature is below the Fermi temperature, which is defined as $\Theta_{\mathrm{F}}=\frac{E_{\mathrm{F}}}{K_{\mathrm{B}}}$, where E_{F} is the Fermi energy and K_{B} is the Boltzmann constant. The Fermi energy at 0 K is given by

$$E_{\mathrm{F}} = \frac{h^2}{2m}\left(\frac{3n}{8\pi}\right)^{2/3}, \tag{4}$$

where m and n represent the mass and number density of the fermions, respectively. According to the Fermi gas model, the total kinetic energy of nucleons is

$$\begin{aligned}\langle E(Z,N)\rangle &= N\langle E_N\rangle + Z\langle E_Z\rangle \\ &= \frac{3}{10m}\frac{\hbar^2}{r_0^2}\left(\frac{9\pi}{4}\right)^{2/3}\left(\frac{N^{5/3}+Z^{5/3}}{A^{2/3}}\right).\end{aligned} \tag{5}$$

It was assumed that the radii of the proton and neutron potential wells are identical. Let $Z-N=\delta$ and $Z+N=A$. By using a binomial expansion, the following re-expression of Eq. (5) near $N=Z$ can be obtained:

$$\begin{aligned}\langle E(Z,N)\rangle = \frac{3}{10m}\frac{\hbar^2}{r_0^2}\left(\frac{9\pi}{8}\right)^{\frac{2}{3}}\Bigg[A + \frac{5}{9}\frac{(N-Z)^2}{A} \\ + \frac{5}{243}\frac{(N-Z)^4}{A^3} + \cdots\Bigg],\end{aligned} \tag{6}$$

which gives us the functional dependence on the neutron surplus. The first term contributes to the volume term in the mass formula, and the second term describes the correction resulting from $N \neq Z$. This so-called symmetry energy increases with the square of the neutron surplus, and the binding energy shrinks accordingly. The third term is the higher order term of the symmetry energy used to improve the semiempirical mass formula. However, the associated coefficients were almost half of the actual values. This deviation arises because only the contributions of kinetic energy and potential energy have not been considered in this calculation.

By adding the fourth-order term of the symmetry energy to the BW2 formula, we obtain the BW3 formula

$$\begin{aligned}BE_{\mathrm{BW3}} = \alpha_{\mathrm{v}}A + \alpha_{\mathrm{s}}A^{\frac{2}{3}} + \alpha_{\mathrm{C}}\frac{Z^2}{A^{\frac{1}{3}}} + \alpha_{\mathrm{t}}\frac{(N-Z)^2}{A} \\ + \alpha_{\mathrm{xC}}\frac{Z^{\frac{4}{3}}}{A^{\frac{1}{3}}} + \alpha_{\mathrm{W}}\frac{|N-Z|}{A} + \alpha_{\mathrm{st}}\frac{(N-Z)^2}{A^{\frac{4}{3}}} \\ + \alpha_{\mathrm{p}}\frac{\delta(N,Z)}{A^{\frac{1}{2}}} + \alpha_{\mathrm{R}}A^{\frac{1}{3}} + \alpha_{\mathrm{m}}P + \beta_{\mathrm{m}}P^2 \\ + b\frac{(N-Z)^4}{A^3},\end{aligned} \tag{7}$$

where

$$b = \frac{1}{162}\left(\frac{9\pi}{8}\right)^{\frac{2}{3}}\frac{\hbar^2}{mr_0^2}. \tag{8}$$

3 Discussion

3.1 Determination of the additional term coefficient

The criteria for evaluating the quality of a semiempirical mass formula hinge on its capacity to embody clear physical principles, minimize dependency on extraction parameters, yield superior calculation results, and clarify the nuclear properties relevant to the nuclear mass. The goodness of fit was assessed using the RMSD of the extraction from the measured binding energies as follows:

$$RMSD = \sqrt{\frac{\sum_i (M_i - F_i)^2}{n}}, \tag{9}$$

where M_i denotes the theoretical value, F_i is the experimental value, and n is the total number of data points.

As discussed above, the value of b calculated using Eq. (8) differs from the experimental fitting value. To obtain an accurate value of b, the following approach was taken: First, Eq. (8) was used to determine the range of b; second, the RMSD of the BW3 mass formula was calculated over the range of b values, with the optimal b value corresponding to the smallest RMSD. The calculations show that the RMSD reaches its minimum value of 1.86 MeV at $b=-1.3$ MeV. Consequently, the value $b=-1.3$ MeV was set in the BW3 mass formula. The fitted coefficients of the semiempirical mass formula in Eq. (7) are provided in Table 1, with the first eleven items aligning with the BW2 mass formula.

To verify the accuracy of the b values, a group of nuclides was randomly selected to create a comparison diagram of the differences between the experimental and calculated values of their specific binding energies. As shown in Fig. 1, the horizontal coordinate represents the range of b values and the vertical coordinate represents the deviation of the specific binding energy between the predicted value of the BW3 mass formula and the experimental value. The BW3 mass formula degenerates into the BW2 mass formula at $b=0$ MeV. It can be observed that all curves for the selected nuclides lie below the origin of coordinates, indicating that the fit of the BW2 mass formula is not ideal. Moreover, if the deviation between the theoretical and experimental values is small, a negative value of b should be adopted. This is because the intersection of the curve with the axis was negative. Figure 1 clearly shows that, when the b value changes between −3 and 3 MeV, the overall trend of the deviation curve is from positive to negative as b traverses from a negative to a positive value. When $b=-1.3$ MeV, the difference in the specific binding energies approaches zero. These results verify that the selection of b is significant.

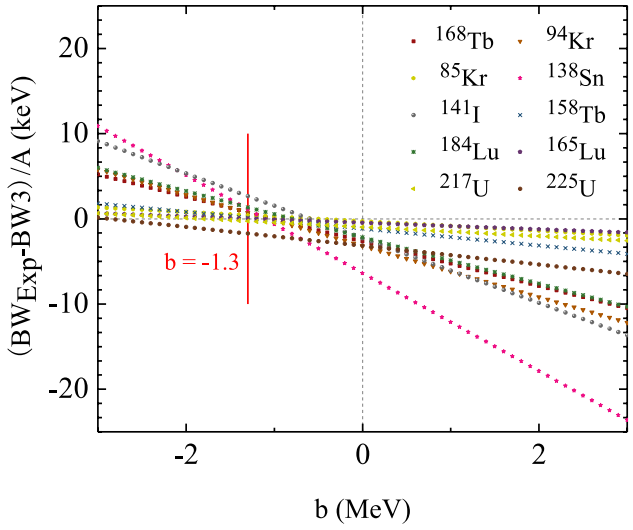

Fig. 1 Deviation of the specific binding energy between the predicted value of the BW3 formula and the experimental value

The nuclide curves for ^{85}Kr, ^{158}Tb, ^{165}Lu, and ^{217}U shown in Fig. 1 are relatively smooth. Although the changes were smooth, they still followed the trend of positive-to-negative deviations in the specific binding energy. The results demonstrate that some nuclides are insensitive to changes in the b value when the BW3 mass formula is used for the prediction. The steepest curve corresponded to ^{138}Sn. At $b = 0$, the deviation was the largest among the selected nuclides. The BW3 mass formula significantly reduces this deviation. For ^{85}Kr, ^{94}Kr, ^{158}Tb, and ^{168}Tb, we can clearly observe that the deviation in the specific binding energy is proportional to the neutron number. When the neutron number was small, the difference changed more gently, and vice versa, becoming steeper. Evidently, an additional term that depends on the difference between the neutron and proton numbers can improve the accuracy of the model for neutron-rich nuclei.

3.2 Effects of the higher order term

Figure 2 shows the difference ($Z, N \geq 8$) between the experimental values of the binding energy and those calculated using the BW2 and BW3 mass formulas. The dotted crosses in the figure indicate that the BW3 mass formula outperforms the BW2 mass formula in this context. By calculating the RMSD for both formulas (i.e., $D_{\mathrm{rms}}^{\mathrm{BW2}} = 1.92$ MeV and $D_{\mathrm{rms}}^{\mathrm{BW3}} = 1.86$ MeV), it is clear that the RMSD of the BW3 mass formula is 3% lower than that of the BW2 mass formula. To analyze the impact of the additional term, a difference distribution between the experimental values of the binding energy and the values calculated from the BW2 and BW3 mass formulas was developed. Local enlargements of $N \approx 95$, $Z \approx 55$ and $N \approx 140$, $Z \approx 83$ are shown in Fig. 2a, b. It is evident from the figures that, for $N \approx 95$ and $Z \approx 55$, the original yellow and orange grids in Fig. 2a are replaced by orange and green grids, respectively, in Fig. 2b. For $N \approx 140$ and $Z \approx 83$, the original yellow, orange, and red grids in Fig. 2a are replaced by green, yellow, and orange grids in Fig. 2b.

The transition from red to green in the color levels set in Fig. 2 indicates a gradual decrease in the difference. This observation shows that the deviation between the predicted value of the nucleus and the experimental binding energy is reduced by the BW3 mass formula. The dotted line crosses the β-stability line, indicating that it lies within a neutron-rich mass region. This observation verified the hypothesis that an additional term can reduce the deviation between the experimental and calculated binding energies of neutron-rich

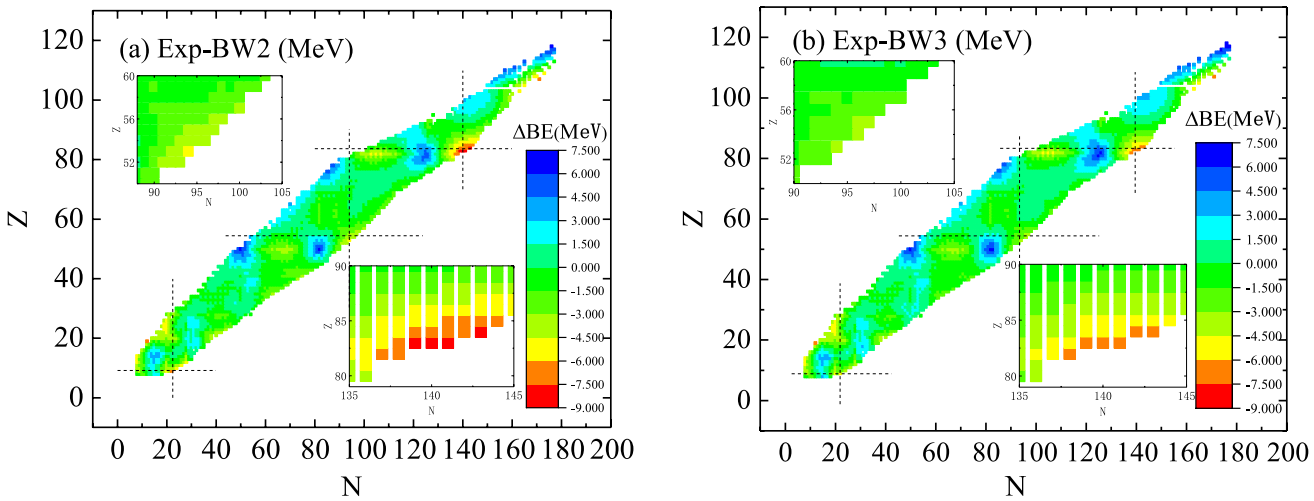

Fig. 2 Deviation from the experimental binding energy of the values predicted by the (**a**) BW2 and (**b**) BW3 mass formulas

nuclei. Simultaneously, for nuclei with magic numbers of protons or neutrons, the deviation between the predictions of the two mass formulas and the experimental data was significant. In the case of double magic nuclei (in which both the neutron and proton numbers are magic numbers), the deviation is particularly pronounced.

To investigate the influence of additional terms on the specific binding energy of neutron-rich nuclei, a group of nuclides and their isotopic chains were randomly selected to calculate the difference between the experimental and calculated specific binding energies obtained from the BW2 and BW3 mass formulas. The isotopic chains of nine types of nuclides were randomly selected, and the deviations between the BW2 and BW3 mass formula predictions and experimental specific binding energies were compared. As shown in Fig. 3, the horizontal coordinate is the neutron number, and the vertical coordinate is the deviation of the specific binding energy. The red curve shows the deviation between the experimental value of the specific binding energy and $BW2_{Theo}$ (calculated value), whereas the black curve shows the deviation between the experimental value of the specific binding energy and the calculated value obtained from $BW3_{Theo}$. As the neutron number increases, the BW3 mass

Table 1 Fit values (in MeV) of the coefficients of the semiempirical mass formula of Eq. (7)

α_v	α_s	α_C	α_t	α_{xC}	α_W
16.58	−26.95	−0.774	−31.51	2.22	−43.40
α_{st}	α_p	α_R	α_m	β_m	b
55.62	9.87	14.77	−1.90	0.140	−1.30

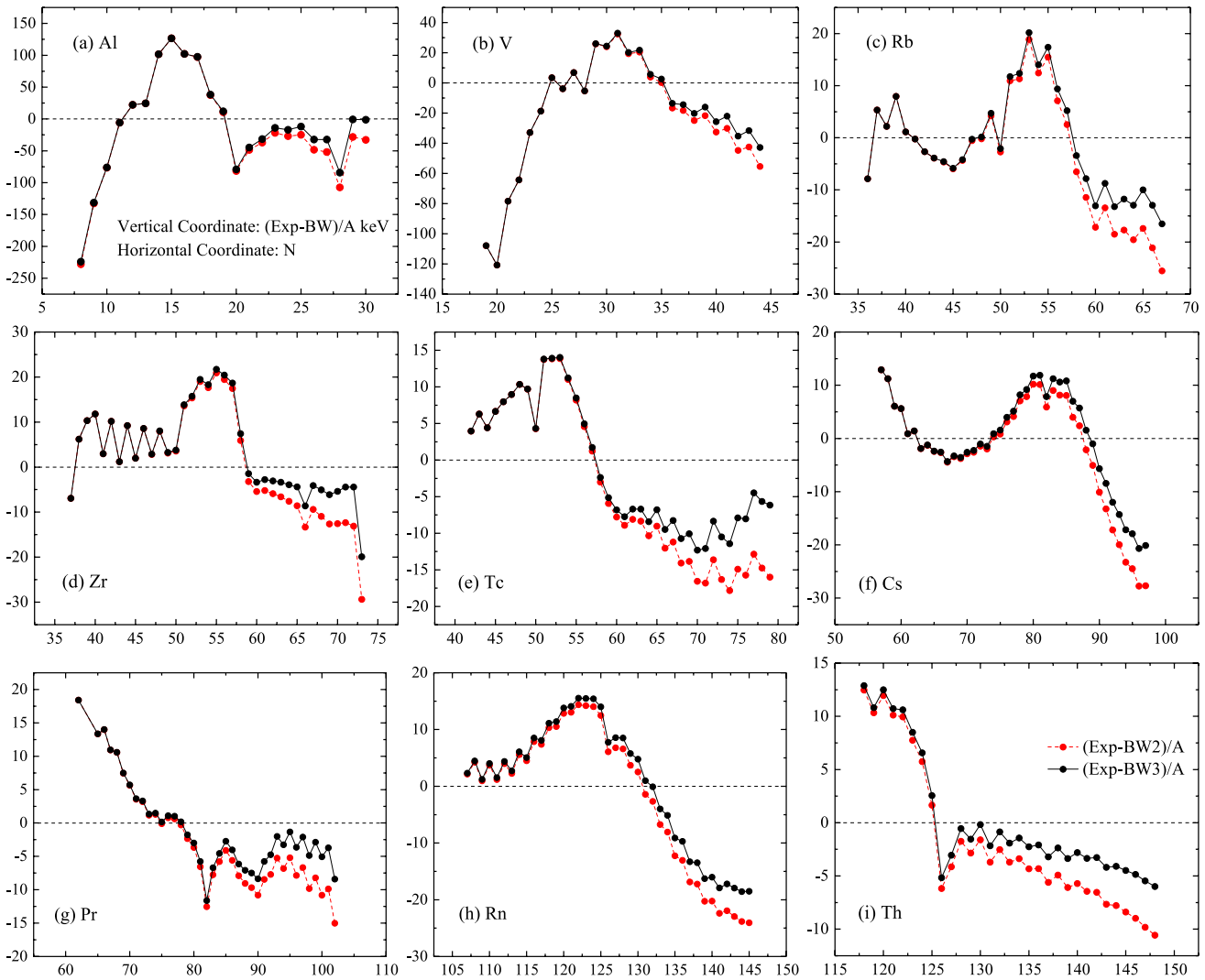

Fig. 3 Differences between the experimental values of the isotope-specific binding energy and the values calculated with the BW2 and BW3 formulas

formula with the additional term (black curve in the figure) improves at the neutron-rich nuclei and exhibits the same trend as that of the BW2 curve. The RMSD decreases to 0.393 MeV when the ratio of the neutron number to the proton number (N/P) is ≥1.6 (RMSD of 2.082 MeV versus 2.475 MeV).

As the neutron number increases, $BW3_{Theo}$ and $BW2_{Theo}$ gradually deviate, and the difference between them increases, particularly for neutron-rich nuclei. The black curve consistently remained above the red curve and approached zero. This trend reveals that the BW3 mass formula can significantly reduce the deviation in the specific binding energies of neutron-rich nuclei. This observation confirms that the BW3 mass formula significantly enhances the calculation accuracy and is more reliable for predicting the mass of neutron-rich nuclei. In Fig. 3, it is apparent that, with a gradual increase in the proton number, the neutron number corresponding to the peak value of the isotope chain curve becomes the magic number. This further indicates that there is a substantial deviation between the predictions of the nuclear mass formula, with the neutron or proton number being the magic number, and the experimental values, implying room for improvement in the mass formula.

3.3 Isobaric elements

To further investigate the predictions of the BW3 mass formula, a comparison graph was developed for six isobaric elements with masses ranging from $A = 100$ to $A = 150$. The graphs in Fig. 4 show the neutron numbers on the horizontal axis and the difference in the specific binding energies on the vertical axis. The red lines represent the deviation between the experimental values of specific binding energy and the calculated values of the BW3 mass formula, and the black lines represent the deviation between the experimental values of specific binding energy and the calculated values of the BW2 mass formula. These six subgraphs reveal that, when the neutron number is small, the two curves almost coincide. This verifies that the difference between the two equations was small at this time; however, as the neutron number increased, the difference between the two equations gradually increased. When the curve intersects the axis, the red curves are completely above the black curves, except for the curve shown in Fig. 4d, indicating that the calculated value of the BW3 mass formula here is closer to the experimental value and is more accurate than the value of the BW2 mass formula.

Because the mass number A is fixed, as shown in Fig. 4, the proton number decreases as the neutron number increases, and the neutron number minus the proton number has a common difference of 2. In particular, the curves in subgraphs in Figs. 4c, d exhibit the steepest trends. In Fig. 4c, when $Z = 46$ and $N = 74$, $|N - Z| = 28$, and the difference in specific binding energy is the closest to zero. The BW3 mass formula is superior to the BW2 mass formula. However, there are also cases in which the difference

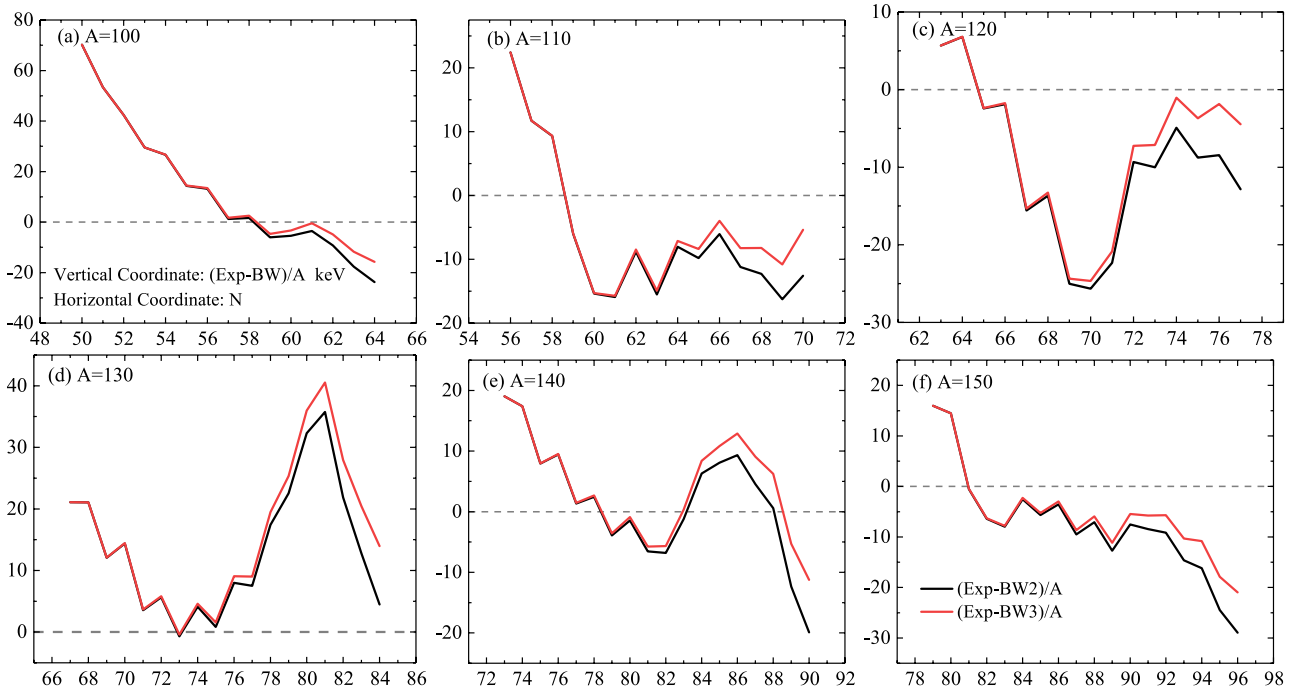

Fig. 4 Differences between the experimental values of the isobaric-specific binding energy and the values calculated with the BW2 and BW3 mass formulas

increases and decreases dramatically, such as $N = 68$ to $N = 69$ and $N = 71$ to $N = 72$. Similarly, in Fig. 4d, at $Z = 57$ and $N = 77$, $|N - Z| = 16$, and the difference in specific binding energy is the closest to zero. However, the calculation accuracy of the BW3 mass formula is close to that of the BW2 mass formula. From $N = 77$ to $N = 81$, the difference in the specific binding energies increased sharply, and the calculation accuracy of the BW3 mass formula was inferior to that of the BW2 mass formula. These trends reveal that there must be a correlation between the remaining terms after removing the volume and surface terms from the mass formula.

4 Summary

In summary, we improved the nuclear mass formula by considering the fourth-order term of the symmetry energy, $b\frac{(N-Z)^4}{A^3}$, in the Fermi gas model. The additional term from the Fermi gas model improved the semiempirical mass formula as the RMSD was reduced by ~3%.

The semiempirical mass formula has a symmetrical energy term $\frac{(N-Z)^2}{A}$ from the Fermi gas model. To extend the mass formula to superheavy nuclei and nuclei far from the β-stability line, we pay special attention to the higher order term $b\frac{(N-Z)^4}{A^3}$ derived from the symmetry energy. The associated coefficients were almost half of the actual values because only the contributions of the kinetic energy and potential energy were not considered in this calculation. The coefficient is derived by fitting the formula to the experimental data. The coefficient was determined when the RMSD reached a minimum value of 1.86 MeV.

To further test the model, the appearance of magic numbers in neutron-rich nuclei was examined. Our results are in good agreement with experimental and theoretical studies. This study demonstrated that our model offered good performance in a neutron-rich mass region, which is useful for rapid neutron capture in nuclear astrophysics. The RMSD decreases to 0.393 MeV when the ratio of the neutron number to the proton number is ≥1.6 (RMSD of 2.082 MeV versus 2.475 MeV).

Author contributions All authors contributed to the study conception and design. Material preparation, data collection and analysis were performed by Xiao-Yu Xu, Li Deng, Ai-Xi Chen, Hang Yang, Amir Jalili, and Han-Kui Wang. The first draft of the manuscript was written by Xiao-Yu Xu and all authors commented on previous versions of the manuscript. All authors read and approved the final manuscript.

Declarations

Conflict of interest The authors declare that they have no Conflict of interest.

References

1. D. Lunney, J.M. Pearson, C. Thibault, Recent trends in the determination of nuclear masses. Rev. Mod. Phys **75**, 1021 (2003). https://doi.org/10.1103/RevModPhys.75.1021
2. N. Wang, Z.Y. Liang, M. Liu et al., Mirror nuclei constraint in nuclear mass formula. Phys. Rev. C **82**, 044304 (2010). https://doi.org/10.1103/PhysRevC.82.044304
3. B.A. Li, L.W. Chen, C.M. Ko, Recent progress and new challenges in isospin physics with heavy-ion reactions. Phys. Rep **464**, 113–281 (2008). https://doi.org/10.1016/j.physrep.2008.04.005
4. W.H. Ye, Y.B. Qian, Z.Z. Ren, Accuracy versus predictive power in nuclear mass tabulations. Phys. Rev. C **106**, 024318 (2022). https://doi.org/10.1103/PhysRevC.106.024318
5. Y.P. Cao, D.H. Liu, Y.B. Qian et al., Uncertainty analysis for the nuclear liquid drop model and implications for the symmetry energy coefficients. Phys. Rev. C **105**, 034304 (2022). https://doi.org/10.1103/PhysRevC.105.034304
6. Y.T. Oganessian, F.S. Abdullin, P.D. Bailey et al., Synthesis of a new element with atomic number $Z = 117$. Phys. Rev. Lett. **104**, 142502 (2010). https://doi.org/10.1103/PhysRevLett.104.142502
7. S. Ćwiok, P.-H. Heenen, W. Nazarewicz, Shape coexistence and triaxiality in the superheavy nuclei. Nature **433**, 705–709 (2005). https://doi.org/10.1038/nature03336
8. A. Sobiczewski, K. Pomorski, Description of structure and properties of superheavy nuclei. Prog. Part. Nucl. Phys **58**, 292–349 (2007). https://doi.org/10.1016/j.ppnp.2006.05.001
9. N. Wang, M. Liu, X. Wu, Modification of nuclear mass formula by considering isospin effects. Phys. Rev. C **81**, 044322 (2010). https://doi.org/10.1103/PhysRevC.81.044322
10. M. Liu, N. Wang, Y. Deng et al., Further improvements on a global nuclear mass model. Phys. Rev. C **84**, 014333 (2011). https://doi.org/10.1103/PhysRevC.84.014333
11. N. Nikolov, N. Schunck, W. Nazarewicz et al., Surface symmetry energy of nuclear energy density functionals. Phys. Rev. C **83**, 034305 (2011). https://doi.org/10.1103/PhysRevC.83.034305
12. G. Audi, A.H. Wapstra, The 1995 update to the atomic mass evaluation. Nucl. Phys. A **595**, 409–480 (1995). https://doi.org/10.1016/0375-9474(95)00445-9
13. G. Audi, A.H. Wapstra, C. Thibault, The Ame 2003 atomic mass evaluation: (II). Tables, graphs and references. Nucl. Phys. A **729**, 337–676 (2003). https://doi.org/10.1016/j.nuclphysa.2003.11.003
14. N. Wang, M. Liu, L. Ou et al., Properties of nuclear matter from macroscopic-microscopic mass formulas. Phys. Lett. B **751**, 553–558 (2015). https://doi.org/10.1016/j.physletb.2015.11.006
15. N. Wang, M. Liu, X.Z. Wu et al., Surface diffuseness correction in global mass formula. Phys. Lett. B **734**, 215–219 (2014). https://doi.org/10.1016/j.physletb.2014.05.049
16. P. Moller, J.R. Nix, W.D. Myers et al., Nuclear ground-state masses and deformations. Atom. Data Nucl. Data Tabl **59**, 185–381 (1995). https://doi.org/10.1006/adnd.1995.1002
17. M.W. Kirson, Mutual influence of terms in a semi-empirical mass formula. Nucl. Phys. A **798**, 29–60 (2008). https://doi.org/10.1016/j.nuclphysa.2007.10.011
18. S. Goriely, N. Chamel, J.M. Pearson, Skyrme-Hartree-Fock-Bogoliubov nuclear mass formulas: Crossing the 0.6 MeV accuracy threshold with microscopically deduced pairing. Phys. Rev. Lett. **102**, 152503 (2009). https://doi.org/10.1103/PhysRevLett.102.152503
19. B.H. Sun, J. Meng, Challenge on the astrophysical R-process calculation with nuclear mass models. Chin. Phys. Lett **25**, 2429–2431 (2008). https://doi.org/10.1088/0256-307X/25/7/027
20. J. Duflo, A.P. Zuker, Microscopic mass formulas. Phys. Rev. C **52**, R23–R27 (1995). https://doi.org/10.1103/PhysRevC.52.R23

21. W.E. Ormand, Mapping the proton drip line up to $A = 70$. Phys. Rev. C **55**, 2407–2417 (1997). https://doi.org/10.1103/PhysRevC.55.2407
22. J. Barea, A. Frank, J.G. Hirsch et al., Garvey-Kelson relations and the new nuclear mass tables. Phys. Rev. C **77**, 041304 (2008). https://doi.org/10.1103/PhysRevC.77.041304
23. J.G. Hirsch, A. Frank, J. Barea et al., Bounds on the presence of quantum chaos in nuclear masses? Eur. Phys. J. A **25**, 75–78 (2005). https://doi.org/10.1140/epjad/i2005-06-050-0
24. C. Ma, M. Bao, Z.M. Niu et al., New extrapolation method for predicting nuclear masses. Phys. Rev. C **101**, 045204 (2020). https://doi.org/10.1103/PhysRevC.101.045204
25. G.J. Fu, H. Jiang, Y.M. Zhao et al., Nuclear binding energies and empirical proton-neutron interactions. Phys. Rev. C **82**, 034304 (2010). https://doi.org/10.1103/PhysRevC.82.034304
26. H. Jiang, G.J. Fu, Y.M. Zhao et al., Nuclear mass relations based on systematics of proton-neutron interactions. Phys. Rev. C **82**, 054317 (2010). https://doi.org/10.1103/PhysRevC.82.054317
27. X. Yin, R. Shou, Y.M. Zhao, Atomic masses of nuclei with neutron numbers $N < 126$ and proton numbers $Z > 82$. Phys. Rev. C **105**, 064304 (2022). https://doi.org/10.1103/PhysRevC.105.064304
28. I.O. Morales, J.C. LópezVieyra, J.G. Hirsch et al., How good are the Garvey-Kelson predictions of nuclear masses? Nucl. Phys. A **828**, 113–124 (2009). https://doi.org/10.1016/j.nuclphysa.2009.07.001
29. N. Wang, M. Liu, Nuclear mass predictions with a radial basis function approach. Phys. Rev. C **84**, 051303 (2011). https://doi.org/10.1103/PhysRevC.84.051303
30. Y.Y. Zong, C. Ma, M.Q. Lin et al., Mass relations of mirror nuclei for both bound and unbound systems. Phys. Rev. C **105**, 034321 (2022). https://doi.org/10.1103/PhysRevC.105.034321
31. C. Ma, Y.Y. Zong, Y.M. Zhao et al., Mass relations of mirror nuclei with local correlations. Phys. Rev. C **102**, 024330 (2020). https://doi.org/10.1103/PhysRevC.102.024330
32. Y.Y. Zong, C. Ma, Y.M. Zhao et al., Mass relations of mirror nuclei. Phys. Rev. C **102**, 024302 (2020). https://doi.org/10.1103/PhysRevC.102.024302
33. E. Alhassan, D. Rochman, A. Vasiliev et al., Iterative Bayesian Monte Carlo for nuclear data evaluation. Nucl. Sci. Tech. **33**, 50 (2022). https://doi.org/10.1007/s41365-022-01034-w
34. Y.Y. Li, F. Zhang, J. Su, Improvement of the Bayesian neural network to study the photoneutron yield cross sections. Nucl. Sci. Tech. **33**, 135 (2022). https://doi.org/10.1007/s41365-022-01131-w
35. Z.P. Gao, Y.J. Wang, Q.F. Li et al., Machine learning the nuclear mass. Nucl. Sci. Tech. **32**, 109 (2021). https://doi.org/10.1007/s41365-021-00956-1
36. X.C. Ming, H.F. Zhang, R.R. Xu et al., Nuclear mass based on the multi-task learning neural network method. Nucl. Sci. Tech. **33**, 48 (2022). https://doi.org/10.1007/s41365-022-01031-z
37. M.R. Mumpower, T.M. Sprouse, A.E. Lovell et al., Physically interpretable machine learning for nuclear masses. Phys. Rev. C **106**, L021301 (2022). https://doi.org/10.1103/PhysRevC.106.L021301
38. R. Utama, J. Piekarewicz, H.B. Prosper, Nuclear mass predictions for the crustal composition of neutron stars: A Bayesian neural network approach. Phys. Rev. C **93**, 014311 (2016). https://doi.org/10.1103/PhysRevC.93.014311
39. R. Utama, J. Piekarewicz, Refining mass formulas for astrophysical applications: A Bayesian neural network approach. Phys. Rev. C **96**, 044308 (2017). https://doi.org/10.1103/PhysRevC.96.044308
40. Z.M. Niu, H.Z. Liang, Nuclear mass predictions based on Bayesian neural network approach with pairing and shell effects. Phys. Lett. B **778**, 48–53 (2018). https://doi.org/10.1016/j.physletb.2018.01.002
41. N.B. Zhang, B.J. Cai, B.A. Li et al., How tightly is the nuclear symmetry energy constrained by a unitary Fermi gas? Nucl. Sci. Tech. **28**, 181 (2017). https://doi.org/10.1007/s41365-017-0336-2
42. H. Yu, D.Q. Fang, Y.G. Ma, Investigation of the symmetry energy of nuclear matter using isospin-dependent quantum molecular dynamics. Nucl. Sci. Tech. **31**, 61 (2020). https://doi.org/10.1007/s41365-020-00766-x
43. R. An, S. Sun, L.G. Cao et al., Constraining nuclear symmetry energy with the charge radii of mirror-pair nuclei. Nucl. Sci. Tech. **34**, 119 (2023). https://doi.org/10.1007/s41365-023-01269-1
44. R. Wang, L.W. Chen, Empirical information on nuclear matter fourth-order symmetry energy from an extended nuclear mass formula. Phys. Lett. B **773**, 62–67 (2017). https://doi.org/10.1016/j.physletb.2017.08.007
45. R. Ogul, N. Buyukcizmeci, A. Ergun et al., Production of neutron-rich exotic nuclei in projectile fragmentation at Fermi energies. Nucl. Sci. Tech. **28**, 18 (2016). https://doi.org/10.1007/s41365-016-0175-6
46. N.B. Zhang, B.A. Li, Astrophysical constraints on a parametric equation of state for neutron-rich nucleonic matter. Nucl. Sci. Tech. **29**, 178 (2018). https://doi.org/10.1007/s41365-018-0515-9
47. Y. Liu, Y.L. Ye, Nuclear clustering in light neutron-rich nuclei. Nucl. Sci. Tech. **29**, 184 (2018). https://doi.org/10.1007/s41365-018-0522-x
48. K. Yoshida, Enhanced moments of inertia for rotation in neutron-rich nuclei. Phys. Lett. B **834**, 137458 (2022). https://doi.org/10.1016/j.physletb.2022.137458
49. B. Jurado, H. Savajols, W. Mittig et al., Mass measurements of neutron-rich nuclei near the $N = 20$ and 28 shell closures. Phys. Lett. B **649**, 43–48 (2007). https://doi.org/10.1016/j.physletb.2007.04.006
50. M. Wang, W.J. Huang, F.G. Kondev et al., The AME 2020 atomic mass evaluation (II). Tables, graphs and references*. Chinese Phys. C **45**, 030003 (2021). https://doi.org/10.1088/1674-1137/abddaf